

The optical design of the Southern African Large Telescope High Resolution Spectrograph: SALT HRS

S. I. Barnes^{a,b}, P. L. Cottrell^b, M. D. Albrow^b, N. Frost^b, G. Graham^b, G. Kershaw^b, R. Ritchie^b, D. Jones^c, R. Sharples^d, D. Bramall^d, J. Schmoll^d, P. Luke^d, P. Clark^d, L. Tyas^d,
D. A. H. Buckley^e, J. Brink^e

^aMcDonald Observatory, University of Texas at Austin, U.S.A.

^bDepartment of Physics and Astronomy, University of Canterbury, N.Z.

^cPrime Optics, Queensland, Australia

^dCentre for Advanced Instrumentation, Durham University, U.K.

^eSouthern African Large Telescope, Observatory, S.A.

ABSTRACT

SALT HRS is a fiber-fed cross-dispersed échelle spectrograph designed for high resolution and high efficiency seeing-limited spectroscopy on the Southern African Large Telescope. The spectrograph, which has a dual channel white pupil design, uses a single R4 échelle grating, a dichroic beam-splitter, and volume phase holographic gratings as cross-dispersers. The échelle grating has 41.6 grooves/mm and is illuminated with a 200 mm diameter beam. This allows $R = 16,000$ with a $2.2''$ fiber and complete wavelength coverage from 370 nm to 890 nm. Resolving powers of $R \approx 37,000$ and 67,000 are obtained using image slicers. The dichroic beam-splitter is used to split the wavelength coverage between two fully dioptric cameras. The white pupil transfer optics are used to demagnify the pupil to 111 mm which ensures that the camera dimensions are kept reasonable whilst also allowing the efficient use of VPH gratings. The spectrograph optics are enclosed inside a vacuum tank to ensure immunity to atmospheric pressure and temperature changes. The entire spectrograph is mechanically and thermally insulated. Construction of SALT HRS began at Durham University's Centre for Advanced Instrumentation in August 2007 and is expected to be complete in 2009. The spectrograph optical design is largely based on work completed at the University of Canterbury's Department of Physics and Astronomy.

Keywords: Spectrograph, high resolution, échelle grating, SALT

1. INTRODUCTION

The high resolution spectrograph (HRS) for the Southern African Large Telescope (SALT) is designed to accomplish a range of observational programs. The primary science drivers for SALT HRS are as follows:

- stellar radial velocity measurements (stellar kinematics, Local Group, extrasolar planets);
- stellar atmosphere analysis (chromospheric activity, seismology, Doppler tomography);
- chemical compositions of stars (abundance analysis, isotopes, nuclear chronometry, SMC/LMC); and
- interstellar and intergalactic absorption (diffuse interstellar bands, Lyman-alpha forest, high redshift absorbers).

The capabilities of SALT HRS will be:

- resolving powers $R \approx 16,000$, 37 000 and 67 000;
- wavelength coverage $\lambda = 370\text{--}890$ nm;
- high mechanical and thermal stability; and
- some limited multi-object capability.

SALT HRS is designed to be competitive with other high resolution spectrographs on large telescopes. For further detail on SALT, and its other instruments see Ref. 1 from this conference.

Corresponding author is Ray Sharples: r.m.sharples@durham.ac.uk

2. THE DESIGN

The spectrograph is a dual beam white pupil design (see Ref. 2), with a single $R4$ échelle grating, a dichroic beam-splitter, and volume phase holographic grating cross-dispersers. The échelle grating has 41.6 grooves/mm and is illuminated with a 200mm diameter beam. Two fully dioptric cameras are used to acquire complete wavelength coverage from 370 nm to 890 nm at a maximum resolving power of $R \approx 67,000$ and in a fixed spectral format. Two objects can be observed simultaneously with a minimum separation of $11''$ between adjacent orders. The higher resolving powers are obtained by using dual fiber image slicers. Apart from shutters, camera focusing, and the fiber interchange mechanism, SALT HRS will contain no moving parts. In order to provide immunity from pressure and temperature changes all optical elements (except the higher resolution fiber feed optics) will be enclosed with a light (~ 2 hPa) vacuum. The entire instrument will in turn be housed in a temperature-stabilized environment. A schematic of the optical layout of SALT HRS is shown in Figure 1.

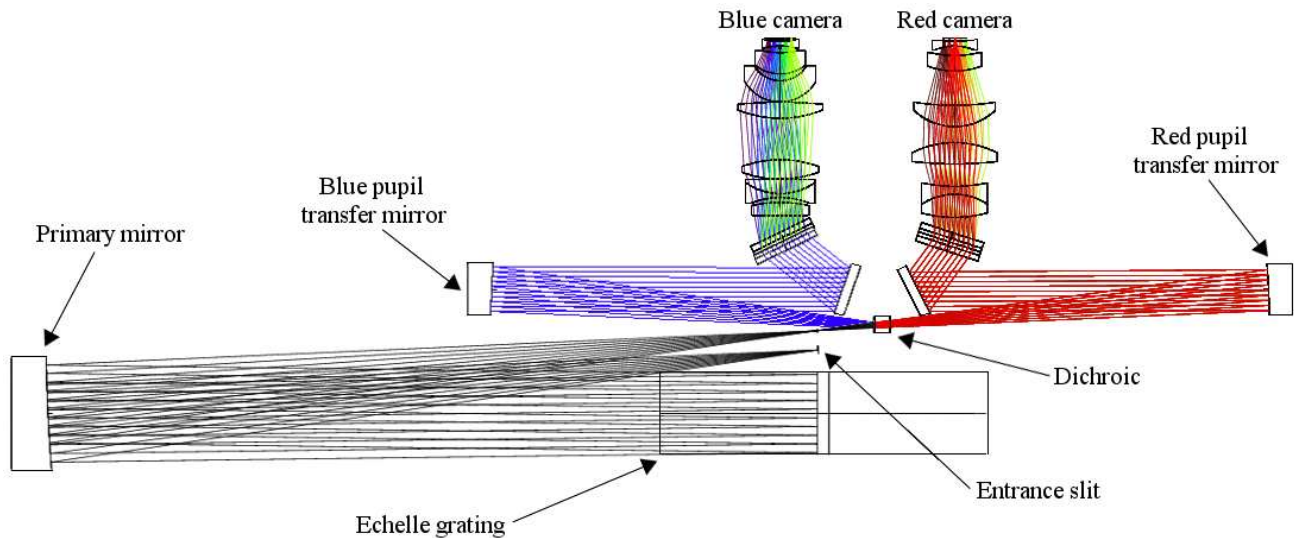


Figure 1. Overview of the Optical layout of SALT HRS. The entrance slit pre-optics are not shown. See text for details.

2.1 The fiber feed

2.1.1 The SALT fiber instrument feed

The SALT Fiber Instrument Feed (FIF) will accommodate up to 12 individual fibers that are mounted in two rows of 6 fibers each. The two rows can be moved apart along a set of rails. A second pair of rails provides motion in the orthogonal direction. Five pairs of fibers are available for use by SALT HRS. Each pair of fibers can be separated anywhere from approximately $15''$ to $1'$. This will limit the variation in vignetting and telecentric angle between the two fibers. To limit reflection losses, the input face of each fiber will be cemented to a fused silica entrance window that will be multi-layer over-coated. A calibration system designed by Swat and Esterhuyse (see Ref. 3) is able to mimic the illumination of the SALT focal plane. The calibration optics can be moved into the beam either immediately prior to or after an observation, or during the daytime. SALT HRS requires at least a thorium argon lamp for wavelength calibration and a white lamp for flat-fielding and échelle order definition.

2.1.2 The fiber modes

At first light, three modes of fiber feeding SALT HRS will be implemented. All three modes will terminate inside the spectrograph vacuum vessel and a moveable mask, placed at the entrance slit, will allow a single mode to be selected. Details of the three fiber feed modes follow:

I) “Fixed object and sky”

In this mode the option of observing one target object and a nearby patch of sky will be possible. Three pairs of fibers will be available:

- i Low resolution ($R \approx 16,000$): $2 \times 500 \mu\text{m}$ ($2.23''$) fibers;
- ii Medium resolution ($R \approx 37,000$): $2 \times 500 \mu\text{m}$ ($2.23''$) fibers with image slicers; and
- iii High resolution ($R \approx 67,000$): $2 \times 350 \mu\text{m}$ ($1.56''$) fibers with image slicers.

It is likely that the bare $500 \mu\text{m}$ fibers will be placed directly at the entrance slit of the spectrograph. Microlenses will be used to produce an $f/3.81$ output beam while also inverting the near and far fields. This helps both the stability and the resolving power of these fibers. The medium and high resolution fibers will be injected into the spectrograph via a set of transfer optics. Further details of the image slicers will be given in Section 2.1.3 below.

II) “Nod and shuffle”

The technique of “nod and shuffle” is widely used in infrared spectroscopy for precise subtraction of the sky background and has been proposed to increase the yield of high density multi-object surveys (see Ref. 4 and Ref. 5). It is also shown (op.cit.) that nod and shuffle spectroscopy would allow much deeper observations on large telescopes such as SALT where the sky emission is significant.

The nod and shuffle mode proposed for the SALT HRS is outlined schematically in Figure 2. It is assumed that the two object spectra can be shuffled so that they overlap in the focal plane, and therefore at the end of a nod and shuffle exposure the spectrum will comprise an object order and two adjacent sky orders. Each of the sky orders will have been captured by the respective fibers. It follows that the observations of the wavelength calibration and flat-fielding sources must be obtained using the same technique. Initially, nod and shuffle will only be available for use at the lowest SALT HRS resolving powers.

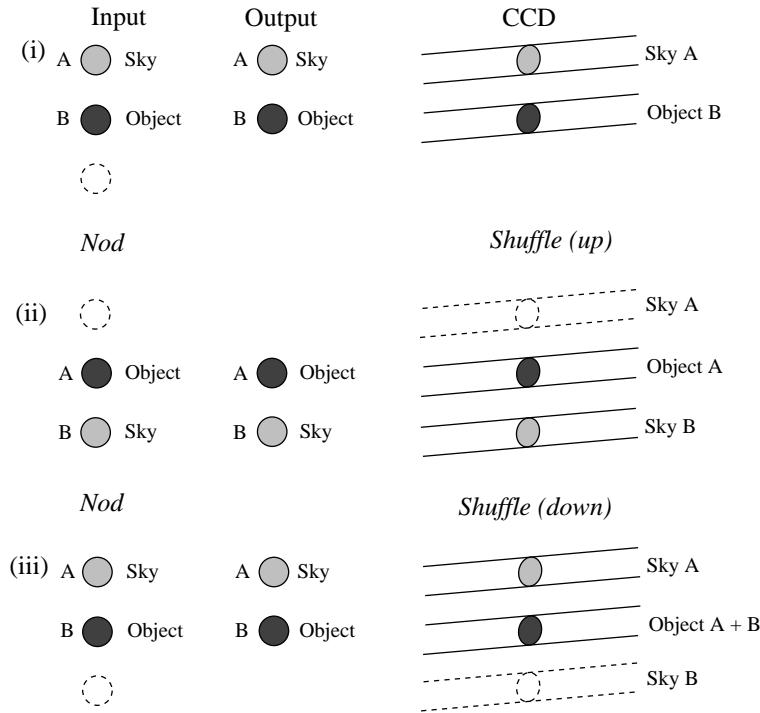


Figure 2. The nod and shuffle concept for fibered spectrographs. (i) Fiber “A” observes the sky while fiber “B” is located on the object. (ii) The telescope is then *nodded* so that fiber “A” captures the object while fiber “B” now observes the sky. To avoid confusing these spectra, the charge on the CCD is *shuffled* upwards so that the object order “A” is now in the position of object order “B” in the previous step. (iii) Next the telescope is *nodded* so that the sky returns to fiber “A” and the object to fiber “B”. The charge on the CCD is shuffled down so that now the object spectra from fibers “A” and “B” overlap.

III) “High stability”

In order to meet the scientific requirements of an ultra high stability mode for Doppler planet searches, a high resolution channel will be added which will include the provision of an iodine cell and simultaneous ThAr calibration. This channel will also include a fiber double scrambler (Ref. 6) and may incorporate a mechanical fiber agitator and/or stretcher to remove any residual spectral modal noise (see Refs. 7 and 8). Since the implementation of these techniques will inevitably impact the optical efficiency of this channel, it has been added as an independent additional mode optimized towards ultra high stability spectroscopy.

2.1.3 Fiber image slicers

A schematic diagram of a proposed image slicer for SALT HRS and the output sliced image are shown in Figure 3. The design is based on a concept by the late R. Bingham (private communication). The slicer will require additional fore-optics in order to convert the $f/3.8$ output of the fibers to the $\sim f/25$ focal ratio required by the image slicer. This slow focal ratio ensures that the defocus is kept to a minimum along the length of the sliced image while also allowing the size of the image slicer to be scaled.

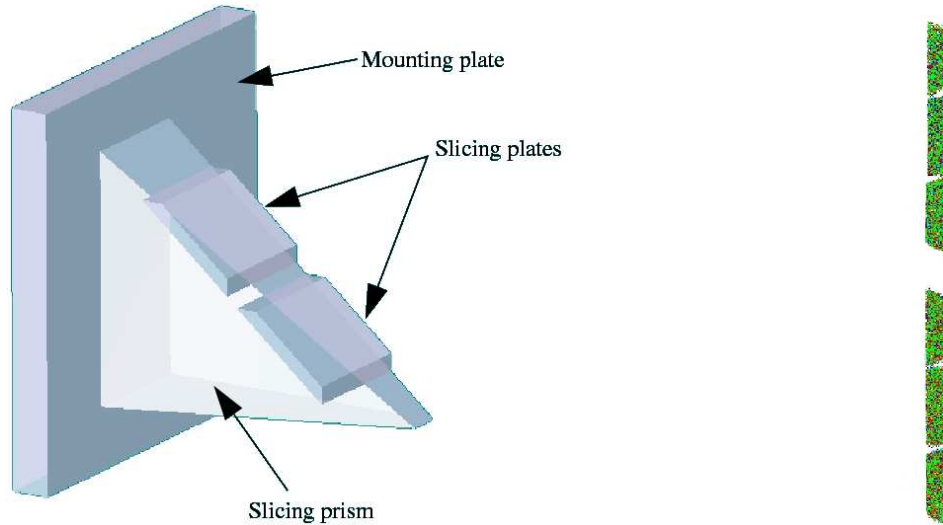


Figure 3. Image slicer concept for SALT HRS (left). The output from a pair of sliced fibers is shown on the right. The design is based on the work of R. Bingham (private communication). It is likely that each slicer plate will in fact have its own slicing prism. This reduces the amount of defocus between the two sliced fibers.

2.2 Primary mirror

The primary mirror (see Figure 1) is used first as a collimator and then, after échelle dispersion, as the first element of a pupil reimager. The mirror is an $f/10$ off-axis paraboloid. This choice of focal length is a compromise between an excessively large instrument (i.e., slow focal ratio), and a tolerably fast focal ratio which can be readily manufactured. In order to accommodate the dual use of the primary mirror as both collimator and as the first pupil transfer mirror, the total aperture must be $270\text{ mm} \times 570\text{ mm}$. The mirror can be sourced from a 690 mm diameter parabolic parent with a 4000 mm radius of curvature.

2.3 Echelle grating

SALT HRS will use a single échelle grating with 41.59 grooves/mm and a 76° blaze angle for primary dispersion. The grating will be formed from a mosaic of two approximately $204 \times 407\text{ mm}$ segments replicated onto the surface of a single $214\text{ mm} \times 840\text{ mm} \times 125\text{ mm}$ Zerodur substrate with a $\sim 15\text{ mm}$ gap between segments. The primary mirror is designed to deliver a 200 mm collimated beam onto the grating, which, assuming fiber focal ratio degradation of 10% , ensures there will be no overfilling. About 5% of incident light will be reflected off an aluminized mylar strip placed between the two grating segments and collected by exposure meter optics. The grating will be illuminated in quasi-Littrow mode; i.e. $\theta = 0^\circ$ and $\gamma \neq 0$. The angle of illumination with respect to the grating facet normal will be approximately $\theta = 0.3 - 0.5^\circ$ *. Following échelle dispersion, the primary mirror is used to form an intermediate image at the mirror's focus.

*The exact value will be determined during commissioning in order to precisely center the blaze function on the CCD. This will also accommodate the tolerance in the grating blaze angle.

2.4 Dichroic

The red and blue arms of SALT HRS are split by a dichroic which is placed 150 mm past the intermediate focus. The nominal wavelength division is 550 nm with a crossover region spanning some 10-15 nm. The orders in which these wavelengths are found are imaged on both spectrograph arms. Splitting allows SALT HRS to make use of a single échelle grating, although the dichroic must then be large enough to cope with an $f/10$ image of the échelle spectrum (i.e., 340×30 mm). The efficiency of the dichroic can be maximized (and the transition region minimized) by limiting the angles of incidence to values near zero, and by using the blue wavelengths in reflection and the red wavelengths in transmission.

2.5 Blue and red pupil transfer mirrors

The blue and red pupil transfer mirrors are used in conjunction with the primary mirror to reimage the pupil from the échelle grating onto the VPH gratings. The focal length of these mirrors is chosen so that the reimaged pupil is 1.8 times smaller than the pupil on the échelle. That is, by using a mirror with a 1111.1 mm focal length the final pupil size will be $200/1.8 = 111.1$ mm (neglecting échelle anamorphism). By demagnifying the pupil, it is possible to significantly decrease the size of the camera optics. However, there are practical limits to the amount of demagnification. The field of view of the camera is inversely proportional to the demagnification. An extremely small camera would require an excessively large field of view and correspondingly more difficult optics (even if they are smaller). Both the blue and red mirrors are identical spherical mirrors (except for their coatings) and each mirror is placed 20 to 30 mm further from the intermediate focus than its focal length. This means that the pupil is not formed in exactly collimated light. To correct for this, the VPH gratings will be immersed in a pair of lenses, and these and the pupil mirrors have been designed as an integrated part of the imaging system. The pupil mirrors will serve as the active focusing element of SALT HRS. The temperature and pressure stability of SALT HRS will limit the need to refocus, and a ± 1 mm shift in pupil mirror focus can compensate for the thermal expansion resulting from a change in temperature from 15 to 25°C. The pupil mirror focus is also needed to compensate for the change in focus from atmospheric pressure to a vacuum. This is possible with a 6.2 mm shift in the blue mirror and a 5.7 mm shift in the red.

2.6 VPH gratings

SALT HRS will use volume phase holographic (VPH) gratings in both the blue and red arms for cross-dispersion. The development of VPH gratings and their potential for use in astronomical instrumentation has been described in Ref. 9. To date, VPH gratings have not been used as cross-dispersing elements in high resolution échelle spectrographs. However, both the proposed SOAR high resolution spectrograph and the PEPSI spectrograph for the LBT are designed with VPH gratings in mind (see Refs. 10 and 11). The parameters of the VPH gratings have been optimized in order to provide the maximum possible order separation while maintaining complete wavelength coverage (given the constraints of finite CCD real estate). The gratings will be located at the white pupil formed by the blue and red pupil mirrors. As was described above, these mirrors demagnify the entrance pupil by a factor of 1.8, and therefore each grating must be ruled a factor of 1.8 denser than if the magnification were unity. This works in favor of VPH gratings since those with low line densities become difficult to manufacture and are potentially less efficient. The blue arm grating will have 1850 lines/mm while the red arm grating will have 855 lines/mm. Both gratings have clear apertures of 134 mm. The grating substrate and cover glasses are both to be made from 10 mm thick pieces of fused silica. Each grating will have matched pairs of plano-concave and plano-convex lenses cemented to their surface. These lenses correct for the slight decollimation at the white pupil. The lenses also allow the spectrograph to avoid recombination ghosts of the type described in Ref. 12. The peak efficiency of each grating should be between 85% and 95%. At the extreme wavelengths of each arm the VPH efficiency should be considerably greater than 50%.

2.7 The cameras

The blue and red arm cameras for SALT HRS are shown in Figures 4 and 5. Both cameras show residual spherical aberration when imaging a perfectly collimated source. This is to be expected because they are optimized (along with the VPH lenses) to balance severe astigmatism and spherical aberration from their second, spherical, pupil mirrors.

The use of a dichroic to split SALT HRS into two beams allows a large number of potential spectrograph formats to be explored. However, as noted above, the efficiency of the dichroic is maximized by limiting the angles of incidence to values near zero. Therefore, in order to avoid a conflict between the blue and red cameras one (or both) spectrograph arms must use at least one additional fold mirror. The layout presented here allows both camera focal planes to be in close proximity to each other which simplifies the mechanical construction.

2.7.1 Blue camera

The blue camera (Figure 4) has a focal length of 166.8 mm. Assuming a detector with $15\ \mu\text{m}$ pixels, this allows for Nyquist (2 pixel) sampling of a maximum resolving power of $R_{\text{max}} = 80,000$. The plate scale is $88\ \mu\text{m}/\text{arcsec}$ (or $11.36\ \text{arcsec}/\text{mm}$). The detector area is $30.7\ \text{mm} \times 61.4\ \text{mm}$ which implies a camera field of view of $\pm 11.6^\circ$ on a diagonal. The first element of the blue camera has a conic surface. This element is made from S-FPL51Y; a glass shared by the third camera lens. The doublet will be formed from PMB2Y/S-FSL5 which have nearly matching coefficients of thermal expansion (CTE). All other elements except the field-flattening lens are to be made from PMB2Y. The field-flattening lens is a singlet made from silica. The lens will be circular and the surface facing the detector is cylindrical. This lens will also serve as the window into the CCD cryostat. The center of the field flattening lens is 6.4 mm from the CCD. All camera elements are coaxial with no tip or tilt. The total path length of the camera is 480 mm, and the maximum lens diameter is 220 mm. Clear apertures will capture 99.5% of all rays assuming a uniform entrance pupil for all wavelengths across a single free spectral range. The wavelength range is from 370 nm to 550 nm.

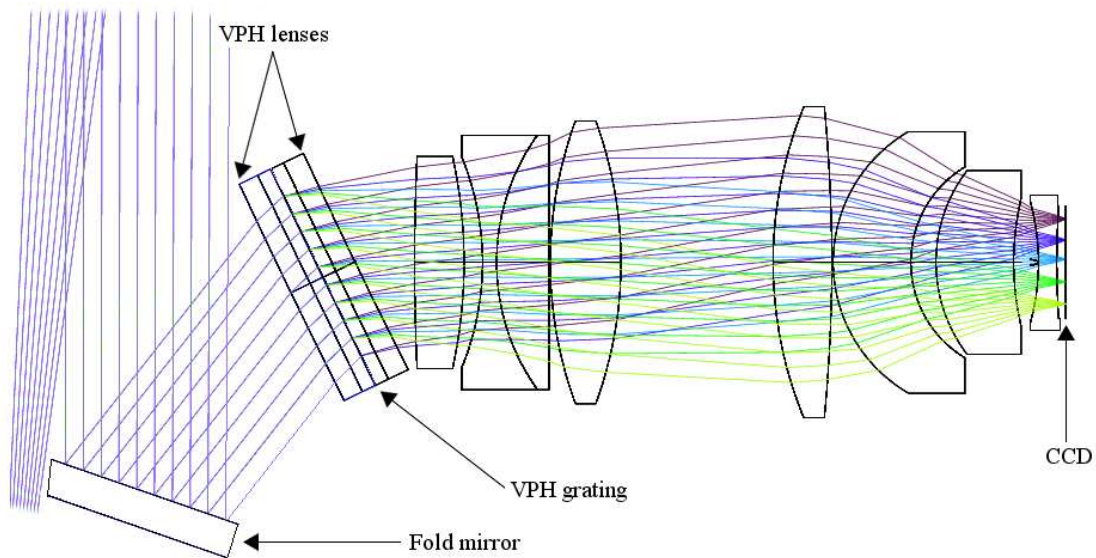


Figure 4. Optical layout of SALT HRS blue camera.

2.7.2 Red camera

The red camera (Figure 5) has a focal length of 208.5 mm. This allows for Nyquist sampling of a maximum resolving power of $R_{\text{max}} = 100,000$, again assuming a detector with $15\ \mu\text{m}$ pixels. The plate scale is $110\ \mu\text{m}/\text{arcsec}$ (or $9.08\ \text{arcsec}/\text{mm}$), and the detector area is $61.4\ \text{mm}$ square. The field of view of the red camera is nearly identical to the blue; that is, $\pm 11.7^\circ$ on a diagonal. Again, the first element of the red camera has a conic surface. The lens also forms part of a cemented S-FSL5/TH1 doublet, where each glass has a matching CTE. The

two largest lenses are formed from S-BAH11 and BK7; both relatively inexpensive glasses. The largest element is 220 mm in diameter. As in the blue camera, the field-flattening lens is made from a single piece of silica with one cylindrical surface located 8.3 mm from the CCD. The red camera field-flattening lens will also be used as a CCD cryostat vacuum window. The total path length through the camera is 470 mm.

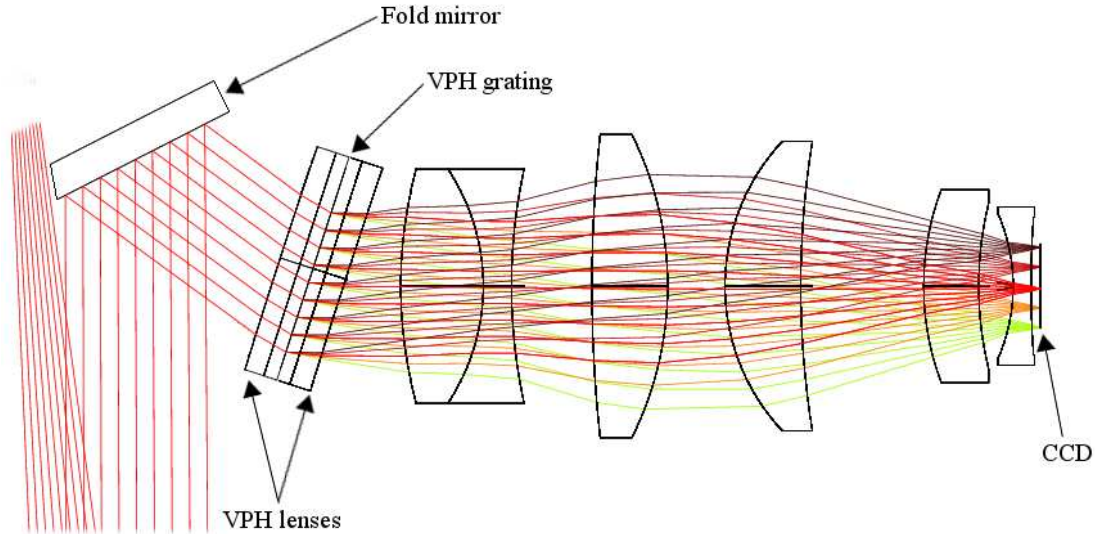


Figure 5. Optical layout of SALT HRS red camera.

2.8 CCDs

The blue arm detector will be a CCD44-82-1-B23 (2k × 4k chip with 15 μm pixels) detector from E2V, thinned and with an AstroBB anti-reflection coating. The red arm will use a CCD231-81-4 (4k × 4k CCD, again with 15 μm pixels) detector also from E2V. This device will use thinned deep-depletion silicon and have an Astro ER1 anti-reflection coating. The detectors will be assembled by Astronomical Research Cameras using Gen III controllers. In order to accommodate a nod and shuffle mode, the cameras must have their columns aligned in the direction of cross-dispersion. The blue camera pixel scale is 5.9 pixels/arcsec (or 0.17 arcsec/pixel) and the red camera pixel scale is 7.3 pixels/arcsec (or 0.14 arcsec/pix).

2.9 Miscellaneous optics

As noted in Section 2.3, a reflective strip placed between the échelle grating segments will be used to provide light to an exposure meter. This is crucial in order to provide correctly weighted times of mid-exposure (for precise barycentric velocity correction), and it will also ensure efficient use of the spectrograph under variable observing conditions. The exposure meter light will be collected by a 150 mm parabolic toroid made from aluminium and directed towards a 6.4 mm fused silica light guide. The coupling efficiency is maximized by placing a cylindrical plano-convex lens on the light guide's entrance. The output of the light guide will illuminate the photocathode of a cooled PMT placed outside the spectrograph's vacuum enclosure.

3. PERFORMANCE

The following sections detail the expected performance of SALT HRS.

3.1 Spectral formats

The red and blue spectral formats are shown in Figures 6 and 7. In both cases, the minimum order separation (for uniquely sampled orders) is above 11". This inter-order space allows for nod and shuffle at the lowest resolving powers (at all wavelengths) and provides sufficient space in which to efficiently slice single fibers for medium and high resolving powers. The wavelength coverage is complete from one order below 370 nm to the order in which $\lambda = 890$ nm is located. The wavelengths in which the dichroic transition occurs are imaged on both detectors.

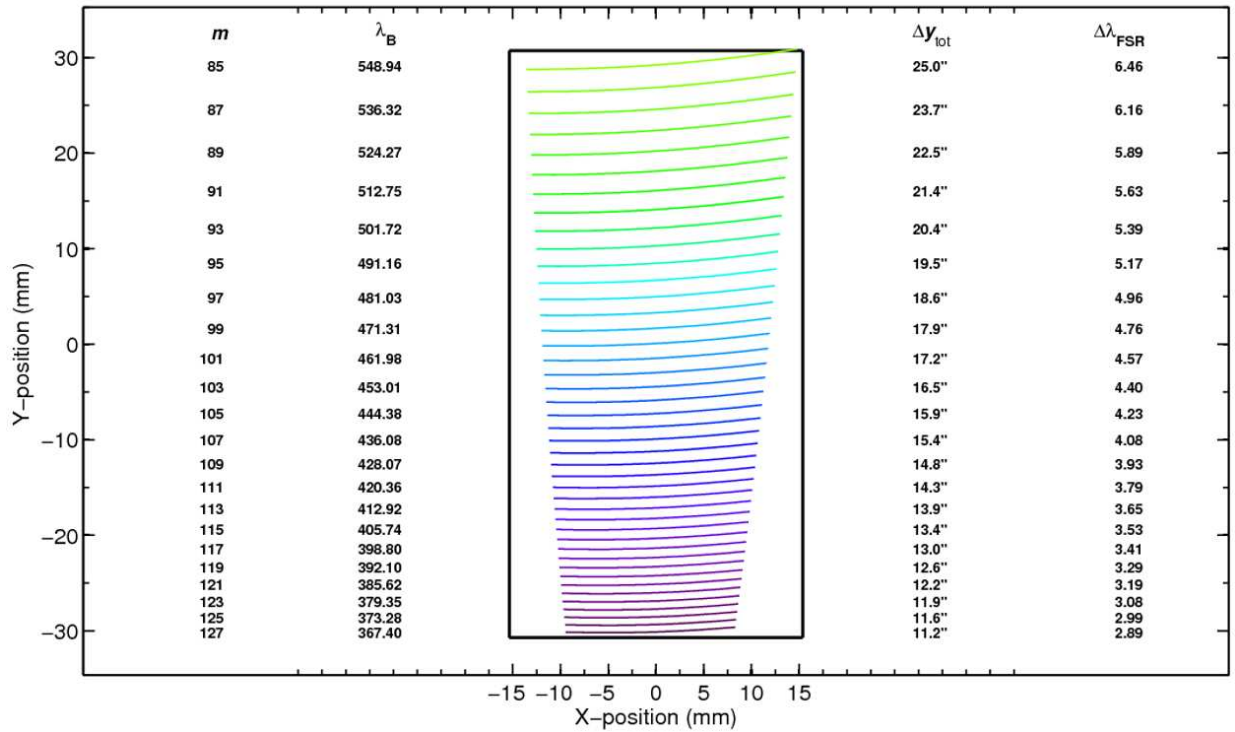


Figure 6. SALT HRS blue spectral format. Each order is traced across one free spectral range. The order number (m), and blaze wavelength (λ_B) are noted. The total inter-order separation (Δy_{tot}) and wavelength extent of each order ($\Delta \lambda_{FSR}$) are also shown. The outline of the CCD is shown in bold.

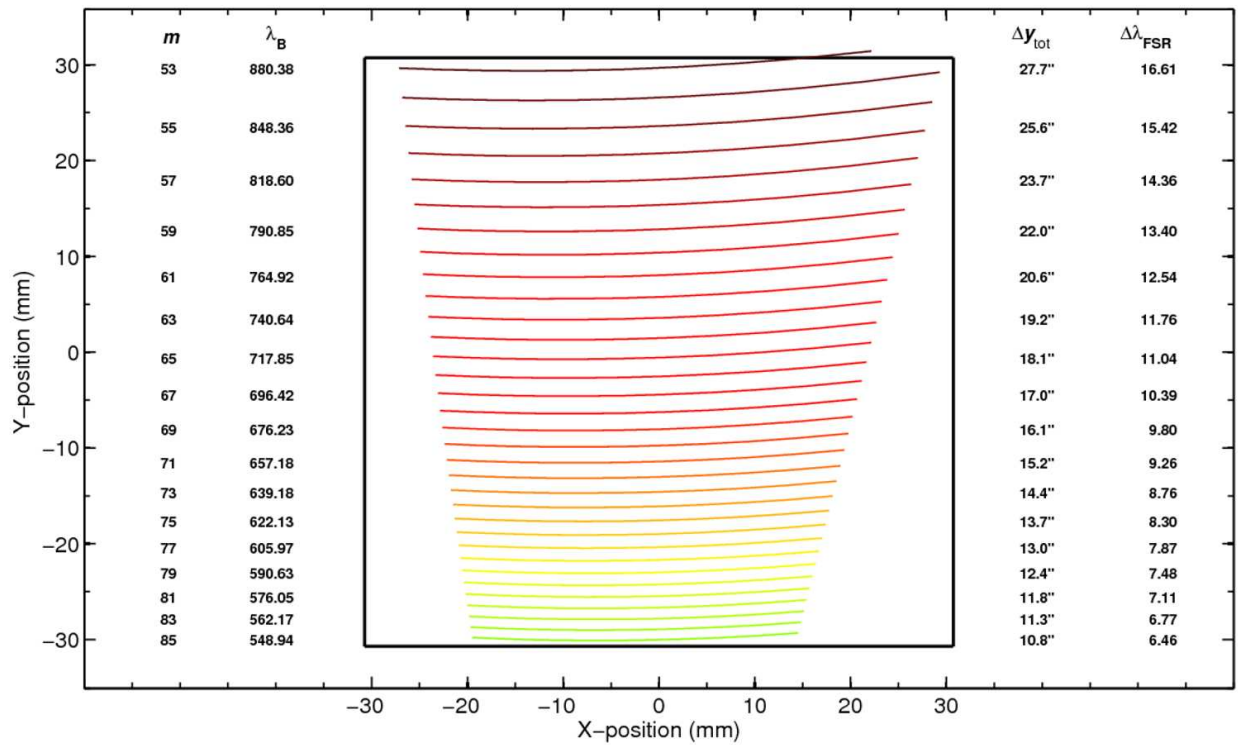


Figure 7. SALT HRS red spectral format. Details are as for Figure 6.

3.2 Image quality and resolving power

3.2.1 Image quality

The image quality of the blue and red arms of the spectrograph is shown in Figures 8 and 9. A detailed analysis of the image quality shows that at all wavelengths from 370 to 555 nm that are within one half a free spectral range from the blaze wavelength, the blue camera ensures that 80% of the encircled energy (EE) is within a box $25 \mu\text{m}$ square. At all these wavelengths, over 50% of the energy is within one pixel. The image quality of the red camera ensures that 80% of the EE being within $25 \mu\text{m}$ square box is met for wavelengths less than 800 nm. The image quality from 800 nm to 890 nm is degraded to approximately $30\text{--}35 \mu\text{m}$ EE(80) diameter.

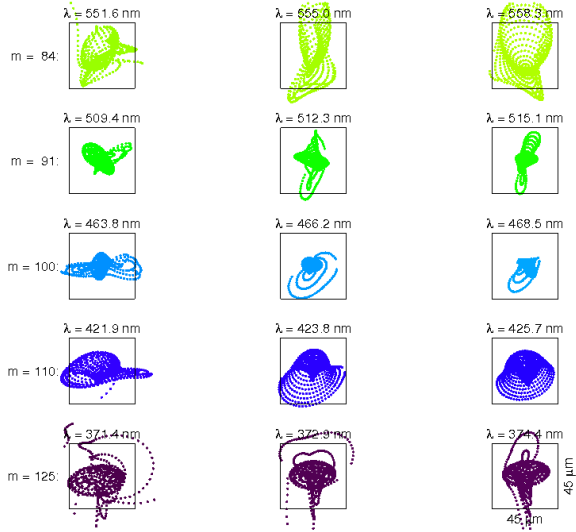


Figure 8. The image quality of the SALT HRS blue arm. Spot diagrams are shown for the middle and ends of orders (one free spectral range only) spread uniformly over the image plane. Wavelengths and order numbers are noted. Each box is three pixels ($45 \mu\text{m}$) square.

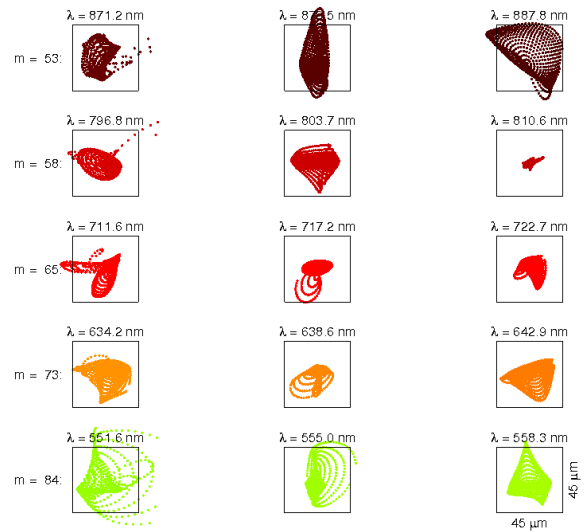


Figure 9. The image quality of the SALT HRS red arm. Details are as for Figure 8.

3.2.2 Resolving power

The resolving power of SALT HRS will not be determined solely by the slit width at the collimator focus. Both the spectrograph's optics and detector will degrade the image of the slit. This will broaden the extracted line spread function of any given spectral line leading to a lower resolving power. The predicted resolving power of SALT HRS has been computed using the method outlined by H. Dekker (private communication) and closely follows the method used for validating the performance of UVES[†]. Details of the resolving power of SALT HRS are given in Table 1. That the spectrograph image quality is sufficient for the highest resolving powers is demonstrated in the synthetic CCD image shown in Figure 10.

Mode	Nominal resolving power ($\lambda/\delta\lambda$)	Fiber diameter (arcsecs)	Slit width (arcsecs)	Effective resolving power ($\lambda/\delta\lambda$)	
				Blue arm	Red arm
Low	16,300	2.23	1.673 ¹	16,200	16,200
Medium	38,400	2.23	0.710	36,600	37,300
High	77,900	1.56	0.355	64,400	69,200

¹The effective slit width of a circular fiber is approximately 0.75 times the full diameter.

Table 1. The resolving power of SALT HRS. The differences in resolving power between the blue and red arms, particularly at the highest resolving powers, are mostly due to the different pixel sampling of a resolution element (see Section 2.7).

[†]http://www.eso.org/observing/dfo/quality/UVES/qc/resolution_qc1.html

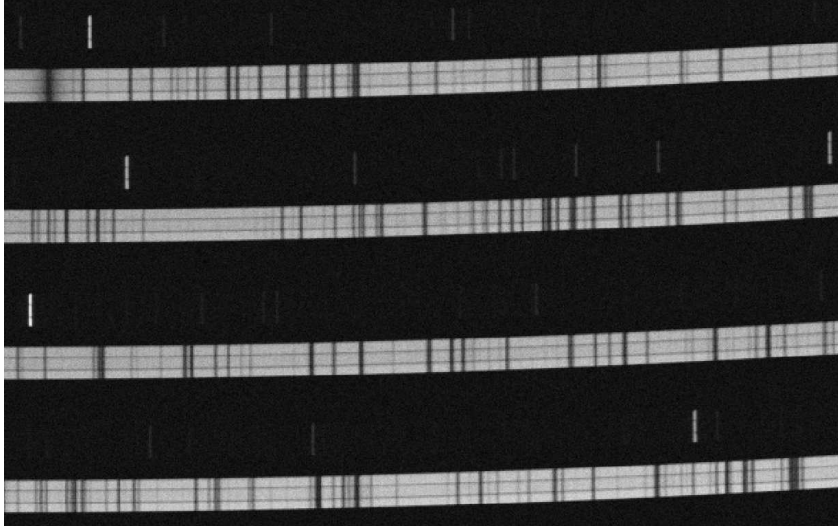


Figure 10. A small section of a synthetic blue arm CCD image. The image in the plane of the CCD has been computed using optical ray-tracing. The main spectrum is of a slowly rotating solar type star, and the second spectrum corresponds to a simultaneous thorium-argon image. The highest resolving power fiber image slicers are assumed.

3.3 Efficiency and signal to noise

3.3.1 Spectrograph efficiency

The predicted efficiencies of SALT HRS are given in the Tables 2, 3 and 4. The spectrograph efficiencies (SPC) include everything except the telescope (TEL) and slit optics (SLT). The slit optics include fibers and, where appropriate, both slit fore-optics and image slicers. The other items are the collimator (COL), which includes overfilling due to focal ratio degradation, the échelle grating (ECH), the cross-dispersers (XDP), the camera (CAM), and the CCD. The camera includes the white pupil mirrors and dichroic.

Details of the efficiency calculations are as follows:

- Telescope – The reflectance of each of the SALT Spherical Aberration Corrector mirror reflectivities are from witness samples made at the time of coating. The primary mirror is standard aluminium. The absorption due to the two elements of the atmospheric dispersion corrector have also been estimated. It is assumed that the mirrors are freshly installed. The telescope image quality is assumed to be $EE(80) = 2.15''$.
- Slit optics and fibers – It is assumed that Polymicro FBP fibers or an equivalent will be used. The fibers are assumed to have overcoated microlenses (or flat windows) at both the input and output. The input losses into each fiber has been calculated assuming $1.12''$ FWHM seeing.
- Image slicers – Geometrical throughputs of $\sim 80\%$ and $\sim 90\%$ are used for the medium and high resolution image slicers, respectively. It is assumed that the throughput of the image slicers is 95% of this value due to scattering and absorption. It is assumed that all transfer optics and windows have efficient multilayer broad band coatings.
- Mirrors – The primary mirror (also the first pupil transfer mirror) is assumed to have a UV enhanced silver coating. The blue and red arm pupil transfer mirrors and fold mirror are assumed to be enhanced aluminium and enhanced silver, respectively. Given the narrow wavelength range over which these mirrors are used, it is possible that these mirrors will in fact have higher efficiency multilayer coatings applied.
- VPH gratings – Data supplied by Wasatch[‡] is used to compute the VPH grating efficiencies. The data is adjusted to allow for the use of multilayer coatings on the VPH lenses.
- Cameras – Standard absorption data are used for each of the camera lens elements. A generic broadband coating has been specified on each element apart from the field-flattening lens which is single layer MgF_2 .
- CCD – The blue arm CCD is assumed to be an E2V 44-82 with a Astro BB coating over standard silicon. The red arm CCD is assumed to be Fairchild 486 which has their broadband overcoat applied. The red arm will actually use a slightly different E2V device, but with similar characteristics and coatings (see Section 2.8).

[‡]<http://www.wasatchphotonics.com>

Wavelength λ (nm)	Order no. m	Component efficiencies (%)								Totals (%)	
		TEL	SLT	COL	ECH	XD	CAM	CCD	SPC	SPC + SLT	SPC + SLT + TEL
379.3	123	60.1	45.8	74.9	56.9	74.4	53.8	67.4	11.5	5.3	3.2
481.0	97	62.3	68.4	91.2	62.3	88.5	77.7	80.3	31.4	21.5	13.4
542.6	86	61.6	72.4	91.0	60.7	66.8	73.1	79.5	21.4	15.5	9.6

Table 2. Efficiencies of the SALT HRS blue arm at the lowest resolving power.

Wavelength λ (nm)	Order no. m	Component efficiencies (%)								Totals (%)	
		TEL	SLT	COL	ECH	XD	CAM	CCD	SPC	SPC + SLT	SPC + SLT + TEL
562.2	83	61.9	73.3	90.8	60.1	85.6	81.7	83.2	31.8	23.3	14.4
648.1	72	59.6	75.1	90.1	58.8	94.5	82.4	94.2	38.9	29.2	17.4
804.5	58	58.8	78.2	89.6	58.2	53.3	81.1	90.3	20.3	15.9	9.4

Table 3. Efficiencies of the SALT HRS red arm at the lowest resolving power.

Fiber mode	Resolving power	Blue arm transmissions (%)			Red arm transmissions (%)		
		SPC	SPC + SLT	SPC + SLT + TEL	SPC	SPC + SLT	SPC + SLT + TEL
Low	16,000	31.4	21.5	13.4	38.9	29.2	17.4
Medium	37,000	31.4	15.1	9.4	38.9	20.3	12.1
High	70,000	31.4	9.6	6.0	38.9	12.9	7.7

Table 4. Efficiency predictions at all resolving powers at a wavelength of $\lambda \approx 650$ nm.

3.3.2 Signal to noise predictions

Using the above efficiency calculations, the signal to noise (S/N) expected for a range of observing conditions has been computed (see Figure 11). In principle, SALT HRS should be capable of obtaining a S/N of 100:1 of a $V = 13.6$ object in 5 minutes at $R \approx 16,000$, where the same limit will be reached for a $V = 15.8$ object after half an hour. Observations of stars around $V = 19$ should allow S/N between 10 and 20 after an hour's exposure.

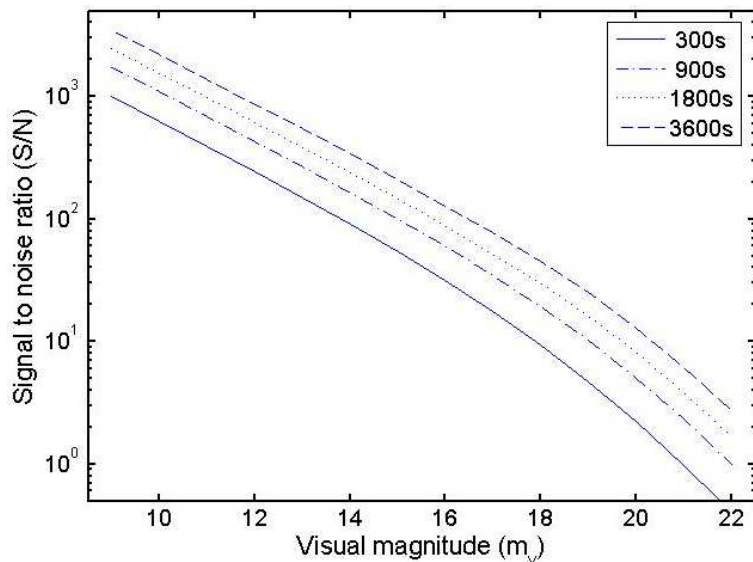


Figure 11. The expected signal to noise ratio (S/N) of SALT HRS as a function of stellar visual magnitude (m_v) and exposure time. The calculations are for a wavelength of 650 nm (i.e., the red arm) and assume the lowest resolving power ($R = 16,000$), a G dwarf star, and a telescope airmass of 1.3. The sky brightness is calculated assuming the moon to be at first quarter. The S/N is for each extracted half-resolution element at the échelle blaze peak.

4. SUMMARY

Construction of SALT HRS is currently underway at the Durham University's Center for Advance Instrumentation[§]. Integration is expected to begin later this year, and it is anticipated that the instrument will be ready for shipping to South Africa by the end of 2009.

[§]see <http://astro.dur.ac.uk/~rsharp/HRS/>

ACKNOWLEDGMENTS

The authors would like to acknowledge the assistance of B. Delabre (ESO) who, in the early stages of this project, described for us the optical concept, not yet published, that had been incorporated in a similar instrument proposed for the SOAR telescope.

REFERENCES

- [1] Buckley, D. A. H., Barnes, S. I., Burgh, E. B., Cottrell, P. L., O'Donoghue, D. E., Nordsieck, K. H., Sharples, R. M., Sheinis, A. I., and Williams, T. B., "Commissioning of the SALT first-generation instruments," *Proc. SPIE* **7014**, these proceedings (June 2008).
- [2] Dekker, H., D'Odorico, S., Kaufer, A., Delabre, B., and Kotzlowski, H., "Design, construction, and performance of UVES, the echelle spectrograph for the UT2 Kueyen Telescope at the ESO Paranal Observatory," *Proc. SPIE* **4008**, 534–545 (Aug. 2000).
- [3] Buckley, D. A. H., Cottrell, P. L., Nordsieck, K. H., O'Donoghue, D. E., and Williams, T. B., "The first-generation instruments for the Southern African Large Telescope (SALT)," *Proc. SPIE* **5492**, 60–74 (Sept. 2004).
- [4] Cuillandre, J.-C., Fort, B. P., Picat, J.-P., and Soucail, G., "Back and forth spectroscopy: optimization of an optical nod-and-shuffle technique to reach fainter objects and increase the multiplex gain on multi-object spectrographs," *Proc. SPIE* **4841**, 1531–1538 (Mar. 2003).
- [5] Glazebrook, K. and Bland-Hawthorn, J., "Microslit Nod-Shuffle Spectroscopy: A Technique for Achieving Very High Densities of Spectra," *Publications of the Astronomical Society of the Pacific* **113**, 197–214 (Feb. 2001).
- [6] Hunter, T. R. and Ramsey, L. W., "Scrambling properties of optical fibers and the performance of a double scrambler," *Publications of the Astronomical Society of the Pacific* **104**, 1244–1251 (Dec. 1992).
- [7] Baudrand, J. and Walker, G. A. H., "Modal Noise in High-Resolution, Fiber-fed Spectra: A Study and Simple Cure," *Publications of the Astronomical Society of the Pacific* **113**, 851–858 (July 2001).
- [8] Chen, C.-H., Reynolds, R. O., and Kost, A., "Origin of spectral modal noise in fiber-coupled spectrographs," *Applied Optics* **45**, 519–527 (Jan. 2006).
- [9] Barden, S. C., Arns, J. A., Colburn, W. S., and Williams, J. B., "Volume-Phase Holographic Gratings and the Efficiency of Three Simple Volume-Phase Holographic Gratings," *Publications of the Astronomical Society of the Pacific* **112**, 809–820 (June 2000).
- [10] Castilho, B. V., Delabre, B., and Gneiding, C. D., "A new concept for echelle spectrographs: the SOAR Telescope Echelle Spectrograph," *Proc. SPIE* **5492**, 433–444 (Sept. 2004).
- [11] Strassmeier, K. G., Woche, M., Andersen, M., and Ilyin, I., "PEPSI: The Potsdam Echelle Polarimetric and Spectroscopic Instrument for the Large Binocular Telescope," *Astronomische Nachrichten* **328**, 627 (July 2007).
- [12] Burgh, E. B., Bershady, M. A., Westfall, K. B., and Nordsieck, K. H., "Recombination Ghosts in Littrow Configuration: Implications for Spectrographs Using Volume Phase Holographic Gratings," *Publications of the Astronomical Society of the Pacific* **119**, 1069–1082 (Sept. 2007).